A Variant Selection Model for Predicting the Transformation Texture of Deformed Austenite

M.P. BUTRÓN-GUILLÉN, C.S. DA COSTA VIANA, and J.J. JONAS

The occurrence of variant selection during the transformation of deformed austenite is examined, together with its effect on the product texture. A new prediction method is proposed based on the morphology of the austenite grains, on slip activity, and on the residual stresses remaining in the material after rolling. The aspect ratio of pancaked grains is demonstrated to play an important role in favoring selection of the transformed copper ($\{311\}\langle 011\rangle$ and $\{211\}\langle 011\rangle$) components. The extent of shear on active slip planes during prior rolling is shown to promote the formation of the transformed brass ($\{332\}\langle 113\rangle$ and $\{211\}\langle 113\rangle$) components. Finally, the residual stresses remaining in the material after rolling play an essential part by preventing growth of the $\{110\}\langle 110\rangle$ and $\{100\}\langle uvw\rangle$ orientations selected by the grain shape and slip activity rules. With the aid of these three variant selection criteria combined, it is possible to reproduce all the features of the transformation textures observed experimentally. The criteria also explain why the intensities of the transformed copper components are sensitive to the pancaking strain, while those of the transformed brass are a function of the cooling rate employed after hot rolling.

I. INTRODUCTION

THE inheritance of preferred orientations during the γ-to-α transformation has been under investigation for a considerable time. Comprehensive reviews of transformation textures have been published recently by Inagaki,[1] Yutori and Ogawa,[2] Ray and Jonas,[3] and Ray *et al.*[4] covering broad aspects of this topic. These surveys have shown that the transformation of austenite to ferrite, martensite, and bainite frequently involves only a restricted set of the 24 possible Kurdjumov–Sachs (K–S) variants. This phenomenon is known as *variant selection* and its origins have been investigated by many authors.

Several different methods have been used to predict the product textures resulting from the γ-to-α transformation. The texture of the γ phase has either been expressed as a discrete set of ideal orientations[5,6] or as a continuous orientation distribution function (ODF). The ODF-based methods require analytical operators to transform the parent texture as a whole; these can be rotation operators, as suggested by Roe[7] and used by Davies *et al.*,[8] or generalized correspondence functions, such as the misorientation distribution function (MODF) proposed by Sargent[9] and used by Bateman and Davies[10] and Davies and Bateman.[11]

While mathematically more efficient, the latter methods are unable to deal with the physical nature of the phase transformation on an individual crystal basis. The discrete orientation methods, on the other hand, allow variant selection mechanisms to be introduced on the level of individual parent orientations, making it possible to investigate the peculiarities of texture transformation in different systems. Of particular interest is the prediction of the transformation textures formed from deformed austenite, especially *pancaked* grains. This is because variant selection observations are generally associated with the deformed microstructures present in microalloyed steels.[12,13] Texture prediction using the K–S relation without variant selection leads to textures that differ qualitatively and quantitatively from those observed experimentally, thus leading to the firm conclusion that some form of variant selection must be taken into account.

Although many variant selection rules have been proposed in a series of attempts to account for the observations, none of these has turned out to be wholly satisfactory.[8,14,15] It was therefore the aim of this investigation to consider some of the selection criteria that have been put forward and, in particular, to suggest that a combination of *three* sets of rules is required in order to remove the discrepancies between predictions and observations.

The three sets of rules are the following: (1) a slip activity-based selection rule; (2) a growth rule based on grain aspect ratio; and (3) a residual stress-based growth condition. Preliminary versions of this model were outlined in the *Hu Memorial Issue of Textures and Microstructures,*[16] as well as in *ICOTOM 11* conference presentations.[17,18,19] The earlier treatment was based on the behavior of *four* of the ideal orientations that characterize the fcc rolling fiber (*i.e.*, the Goss, brass, S, and copper). Here, three further orientations are taken into consideration (*i.e.*, the Goss-brass, brass-S, and S-copper, which are defined in greater detail subsequently), and the model is demonstrated to apply to all *seven* of the characteristic rolling fiber components. In the sections that follow, the model is described and shown to be capable of predicting the transformation textures that result from the fcc-to-bcc transformation.

M.P. BUTRÓN-GUILLÉN, formerly Research Associate, Department of Metallurgical Engineering, McGill University, is Visiting Professor, Military Institute of Engineering, 270 Rio de Janeiro-RJ, Brazil. C.S. DA COSTA VIANA, Professor, is with the Instituto Militar de Engenharia, IME. J.J. JONAS, Professor, is with the Department of Metallurgical Engineering, McGill University, 3610 University St., Montreal, PQ, Canada H3A 2B2.

Manuscript submitted November 21, 1996.

Table I. Principal Characteristics of the Bain, K–S, and N–W Relations

Orientation Relationship	Lattice Correspondence Relation	Number of Alternatives	Total Number of Variants
Bain	{001} ‖ {001}	3	3
	⟨100⟩ ‖ ⟨110⟩	1	
K–S	{111} ‖ {011}	4	24
	⟨011⟩ ‖ ⟨111⟩	3	
	(twin-related variants)	2	
N–W	{111} ‖ {011}	4	12
	⟨112⟩ ‖ ⟨011⟩	3	

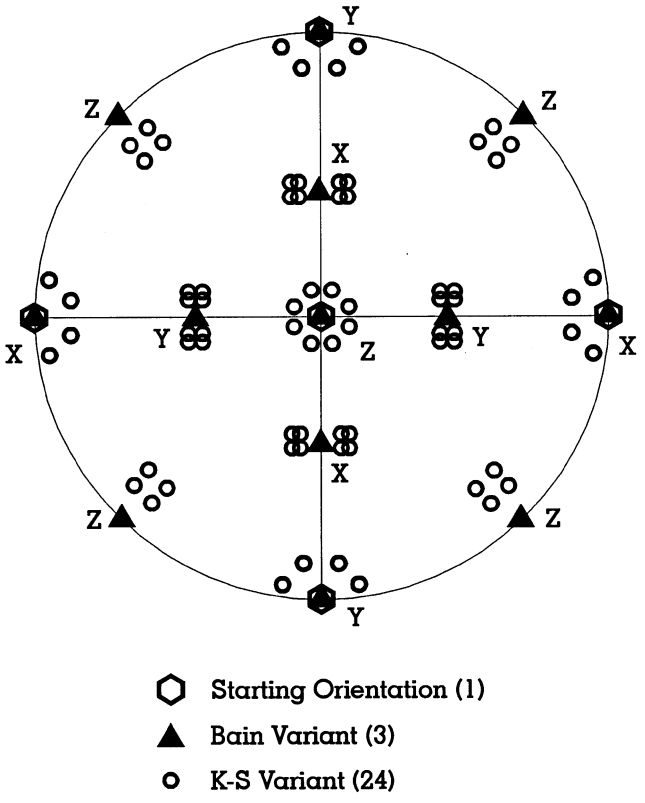

Fig. 1—Schematic representation of the parent cube orientation, the three Bain product variants, and the 24 corresponding K–S variants.

II. ORIENTATION RELATIONSHIPS BETWEEN γ AND α: TEXTURE INHERITANCE

When austenite transforms to ferrite, martensite, acicular ferrite, or bainite, similar textures are produced, despite the fact that ferrite is formed by diffusion, martensite by a shear mechanism, and acicular ferrite and bainite by a mixed mode. Several orientation relationships have been proposed for this type of transformation, including the ones suggested by Bain,[20] Kurdjumov and Sachs,[21] and Nishiyama[22] and Wassermann[23] (N–W). Experimental evidence indicates that the K–S relation is generally followed in these cases, although the validity of the N–W relation has also been demonstrated.[8,24] The principal characteristics of the Bain, K–S, and N–W relations are given in Table 1.

When austenite is rolled at high temperatures, *i.e.*, above the austenite no-recrystallization temperature, T_{nr}, a recrystallization texture is formed, the strongest component of which is the cube orientation {001}⟨100⟩.[1] This transforms to the rotated cube {100}⟨011⟩, Goss {110}⟨001⟩, and rotated Goss {110}⟨110⟩.[1,4] If, however, the austenite is unable to recrystallize before transformation, it retains the relatively sharp deformation texture that forms during rolling; the latter contains the brass {110}⟨112⟩, copper {112}⟨111⟩, and S {123}⟨634⟩ as main components, with the Goss {110}⟨001⟩ as a minor component. The major orientations of the resulting product texture are the {332}⟨113⟩ and {113}⟨110⟩, which originate from the brass and copper components, respectively.[4,21]

The presence of rotated cube, Goss, and rotated Goss in the ferrite formed from *recrystallized* austenite can be readily explained in terms of the geometries of the Bain and K–S relationships. The most important single texture component in recrystallized austenite is the cube {100}⟨001⟩. A rotation of 45 deg about either the ND, RD, or TD ⟨100⟩ axis (*i.e.*, the ⟨100⟩ axis which is parallel to the normal, rolling, or transverse direction, respectively), as called for by the Bain transformation, leads directly to the rotated cube, Goss, and rotated Goss orientations, respectively.[4,25] A similar result is obtained from the K–S transformation, except that each of the three Bain variants is replaced by eight K–S variants, distributed symmetrically at a distance of 11.06 deg about each Bain variant.[4,25]

The relations between the parent cube orientation, the three Bain product variants, and the 24 K–S product variants are depicted in Figure 1.[4,25] The predictions of the two sets (Bain and K–S) of transformation relations (as well as those of the N–W relationship) are in fairly good agreement with experimental observations for recrystallized austenite, and so will not be considered further here.

III. THE MODEL

A. *Rotation Axes for Variant Selection*

In the present model, it is assumed that the material is elastic/ideally plastic and that all the austenite grains are in the deformed condition, *i.e.*, unrecrystallized, immediately prior to transformation. It is considered that the orientation relationship between the two phases is described by the K–S[21] relation, and that this can be represented by a plus or minus 90 deg rotation about a ⟨112⟩ axis common to both lattices.

According to the model, the K–S correspondence relations that define the orientations of the nuclei are expressed in terms of the {111} slip planes and ⟨110⟩ slip directions of the parent fcc material using the geometry described by Bishop and Hill.[26] Each correspondence plane and direction is in turn linked to the particular ⟨112⟩ rotation axis that relates the parent and product grains. The indices of this axis are obtained from the cross-product of the plane normal and slip direction that make up the fcc slip system.

The notation employed to describe the {111}⟨110⟩ slip systems and the respective ⟨112⟩ rotation axes is presented in Table II. One-half of the octahedron formed by the full set of {111} planes is illustrated in Figure 2; the remaining 12 ⟨110⟩ and ⟨112⟩ directions are the negatives of the ones presented in this diagram. It should be noted that a −90 deg rotation about the [112] axis, for example, is equivalent to a +90 deg rotation about the $[\bar{1}\bar{1}\bar{2}]$ axis.

Embedded in the correspondence relation described pre-

Table II. Slip Systems, as Defined by Bishop and Hill,[26] and Their Associated ⟨112⟩ Axes

Plane or Axis	Slip System and Corresponding ⟨112⟩ Rotation Axis											
	a (111)			*b* ($\bar{1}\bar{1}1$)			*c* ($\bar{1}11$)			*d* ($1\bar{1}1$)		
{111}	I	II	III	I	II	III	I	II	III	I	II	III
⟨110⟩	$[01\bar{1}]$	$[\bar{1}01]$	$[1\bar{1}0]$	$[0\bar{1}\bar{1}]$	[101]	$[\bar{1}10]$	$[01\bar{1}]$	[101]	$[\bar{1}\bar{1}0]$	$[0\bar{1}\bar{1}]$	$[\bar{1}01]$	[110]
⟨112⟩	$[2\bar{1}\bar{1}]$	$[\bar{1}2\bar{1}]$	$[\bar{1}\bar{1}2]$	$[\bar{2}1\bar{1}]$	$[1\bar{2}\bar{1}]$	[112]	[211]	$[\bar{1}\bar{2}1]$	$[\bar{1}1\bar{2}]$	$[\bar{2}\bar{1}1]$	[121]	$[1\bar{1}\bar{2}]$

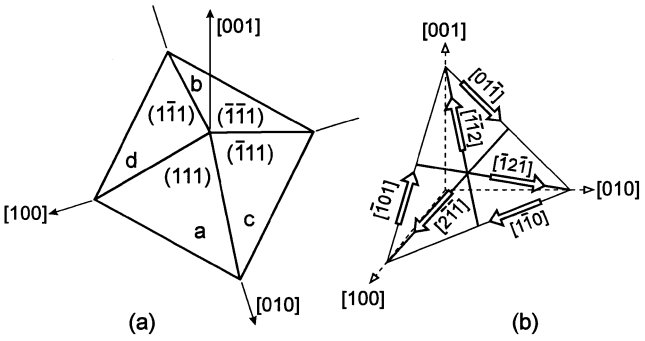

Fig. 2—(*a*) One-half of the octahedron formed by the {111} planes employed in the Bishop–Hill[26] notation. (*b*) The ⟨110⟩ and ⟨112⟩ directions associated with plane ''a.''

viously is an important basic assumption of the present model: that the principal direction of product growth, *i.e.*, the one along which the transformation interface propagates, is an fcc ⟨111⟩ direction. This assumption finds support in the work of Kelly and Nutting[27] and of Altstetter and Wayman,[28] who have shown that low carbon martensites (and even that formed from pure iron) display apparent {111}-fcc habit planes and contain laths that are parallel to the ⟨110⟩ directions lying in those planes.

As the model is concerned with nucleation in *deformed* materials, the effect on variant selection of the slip activities involved in the final rolling deformation step is of particular importance. The 12 slip systems that define the variants can be classified as *active* or *inactive*; in the former case, it is possible to calculate their respective shear rates. Thus, tables of relative slip activity can be drawn up, and these can be used in turn to select the most active, second most active, *etc.*, slip systems. The latter information can then be used to identify the variants that are favored by slip activity considerations.

Predictions of the K–S theory without variant selection; comparison with experimental observations

The 24 K–S relations were first used to calculate the transformation texture expected to form from deformed austenite when variant selection is not taken into account. To represent the texture of pancaked austenite, seven orientations were selected from the orientation tube developed in the plane strain rolling of fcc materials. These are the Goss, Goss-brass, brass, brass-S, S, S-copper, and copper; their respective locations in Euler space are listed in Table III. The volume fraction assigned to each parent orientation was based on the experimental intensities associated with the texture tube determined on a 95 pct cold-reduced Ni-30 wt pct Co alloy.

Each of these orientations was transformed on an individual basis by rotating it by plus or minus 90 deg about

Table III. Locations in Euler Space of the Seven Selected Parent Orientations

Orientation	φ_1	Φ	φ_2
Copper	90.0	35.26	45.0
Copper–S	74.0	36.0	54.0
S	58.98	36.7	63.43
S–Brass	46.12	34.5	75.96
Brass	35.26	45.0	90.0
Brass–Goss	15.79	45.0	90.0
Goss	0.0	45.0	90.0

the ⟨112⟩ axes listed in Table II. Since each parent orientation generates 24 product nuclei, its initial volume fraction was shared equally among the respective product orientations. The latter were fitted with Gaussian functions (θ_0 = 8 deg), which were then superimposed and added to a uniform ''background'' distribution of bcc orientations, which represent the background in the parent austenite. For the present purpose, volume fractions of 60 pct fiber components and 40 pct background components were generally used.

The texture of the parent material is illustrated in Figure 3(a), while that of the product resulting from the preceding ''no-variant'' calculation is presented in Figure 3(b). Here, ϕ_2 = 45 deg diagrams are employed, and the ideal orientations located in this cross section are identified in Figure 3(c). The parent texture is both qualitatively and quantitatively similar to that determined on a 90 pct cold-rolled Fe-30 wt pct Ni alloy by Bateman and Davies.[10] Their experimental martensite texture is therefore reproduced here as Figure 4(a) for comparison with the simulated product texture of Figure 3(b). Also of interest is a texture that typifies the behavior of the pancaked Nb steels that transform to ferrite and pearlite on air cooling; an example of such a texture is reproduced here as Figure 4(b).[13] When higher cooling rates are employed in Nb-containing steels, either bainitic[29] or martensitic[30] microstructures are formed. Examples of the textures associated with these two additional types of steel products are presented in Figures 4(c) and (d).

Several detailed conclusions can be drawn from these figures by identifying the main components that are absent, as well as those that are present, together with their relative intensities.

The ⟨110⟩‖TD component (that which has a ⟨110⟩ direction parallel to the transverse direction) located along the lower right-hand side of the ODF is the {332}⟨113⟩, which is usually referred to as the transformed brass component.[25] (This has also been indexed as an approximate {111}⟨112⟩ orientation.[4,13]) By comparing the K–S predictions (Figure 3(b)) with the experimental data (Figure 4), it

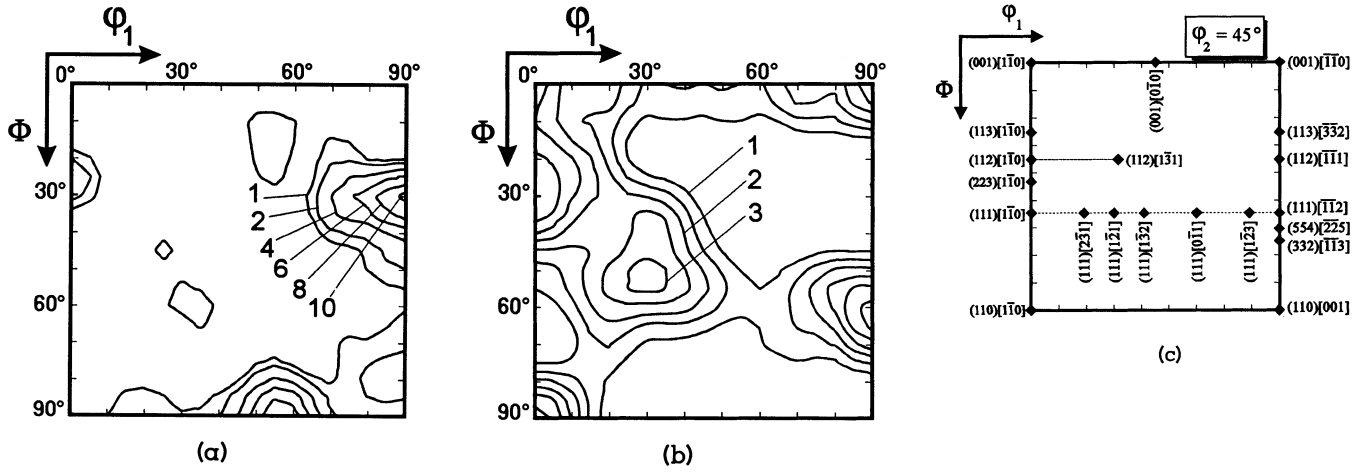

Fig. 3—(*a*) Texture of the parent (fcc) material. (*b*) Product (bcc) texture, after no-variant calculation. (*c*) Ideal orientations in the φ_2 = 45 deg ODF section.

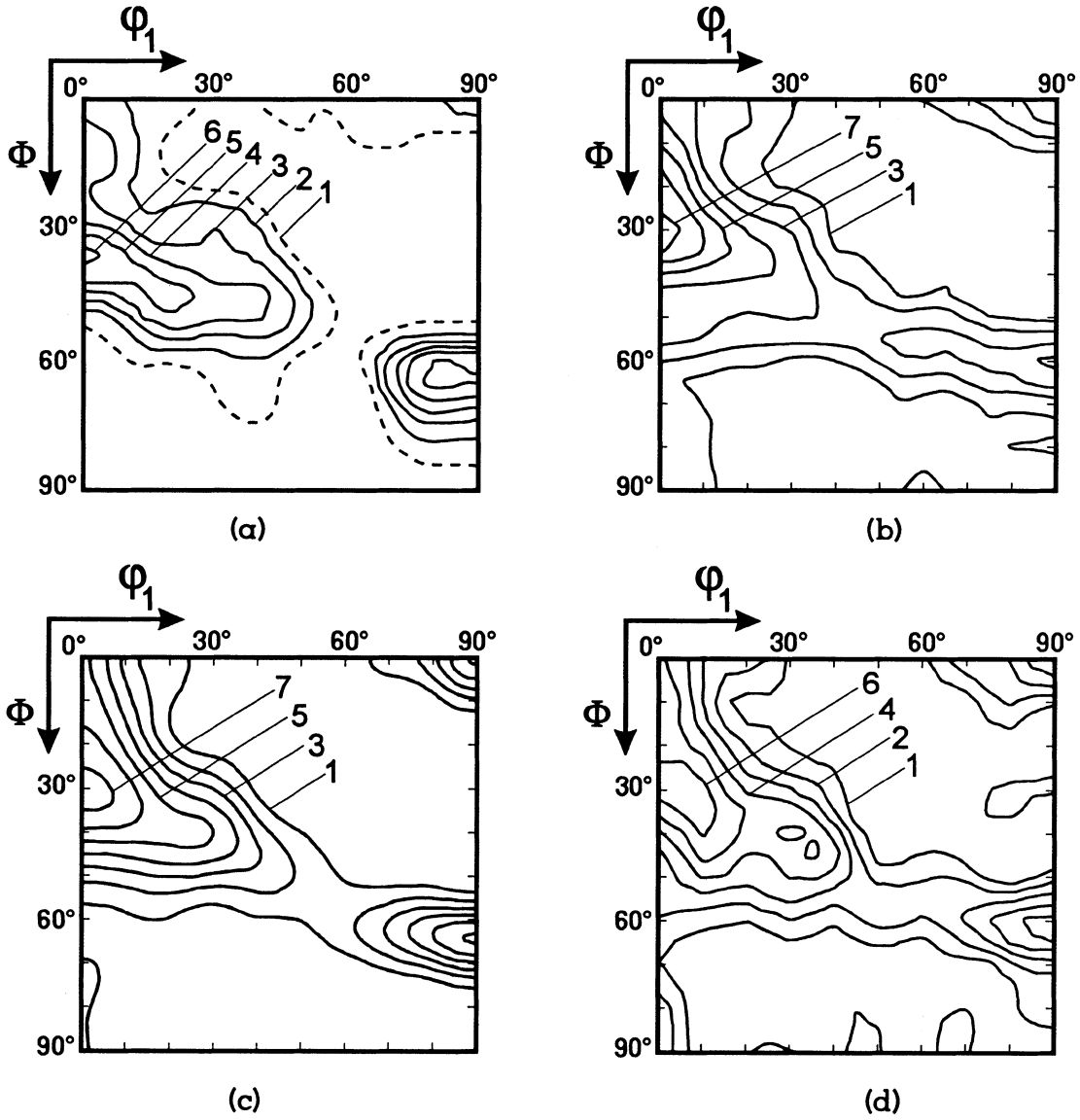

Fig. 4—(*a*) Experimental martensite texture of Bateman and Davies.[10] (*b*) Ferrite/pearlite transformation texture of a pancaked Nb steel.[13] (*c*) Bainite transformation texture of a pancaked Nb steel.[29] (*d*) Martensite transformation texture of a pancaked Nb steel.[30]

is readily evident that the observed transformed brass component intensities are nearly twice as high as in the simulations. This generalization remains valid when the background volume fraction is reduced progressively from 40 (Figure 3(b)) to 30 pct and even 15 pct. (The latter two simulations are not presented here.)

We turn now to the intensities of the {211}-{311}⟨011⟩ or transformed copper components, located on the left side of the ODF and forming part of the ⟨110⟩‖RD fiber (orientations with a ⟨110⟩ axis parallel to the rolling direction). Here, the experimental peak intensities are more than twice the maximum displayed in the predicted texture (Figure 3(b)). These two components are observed in the presence of pancaked grains (*i.e.*, grains with high aspect ratios) and therefore when finish rolling is completed below the T_{nr}. (A similar observation was made by Inagaki[1] in 1978.) Another important difference between Figures 4 and 3(b) concerns the {110}⟨110⟩ orientation (lower left corner). This is generally absent, or almost absent, in experimental textures.

It is therefore clear that some form of variant selection must be employed in texture prediction if the transformation is to be simulated properly. Similar conclusions were drawn recently by Brückner *et al.*[31]

B. *Effect of Slip Activity*

Here, the seven orientations mentioned previously, *i.e.*, the Goss, Goss-brass, brass, brass-S, S, S-copper, and copper, were again chosen to represent the austenite texture.[30] As mentioned earlier, the slip systems that define the variants can be classified according to their relative activities. For this purpose, the rate-sensitive slip analysis of Zhou *et al.*[32] was employed. Plane strain compression was considered to take place and the shears occurring on the active systems were calculated, based on a von Mises incremental strain of 0.025. The results obtained in this way can be used to rank the various nucleus orientations in the order of their slip activities.

To this end, the normalized shears were divided into four categories. The first three categories are all associated with the *active* planes: these are referred to here as (1) most active, (2) second most active, and (3) low or nil activity. Nil corresponds to an inactive *direction* on an active *plane*. The fourth category corresponds to the variants associated with slip directions that lie in planes that are *not activated at all*. The preceding classification is the basis of a selection rule that assigns weights (or probabilities) to products as functions of the slip activities observable in the parent phase.

This rule was applied to the seven ideal orientations listed earlier. The full list of bcc product orientations is displayed in Table IV, together with the 24 rotation axes and corresponding slip systems. The products are identified by sets of low integer Miller indices lying within 11 deg of the exact orientations. In the present case, the maximum shear activity is 1.66, all values having been normalized with respect to the 0.025 incremental strain mentioned previously. In the case of the 'nil' category, the symbol ''0'' refers to an inactive direction lying in an active plane. The symbol ''000'' represents an inactive system lying on a totally inactive plane. (The orientations associated with the latter systems are analyzed in greater detail subsequently.)

The orientations of the variants associated with the slip systems that lie in active planes in each of the seven fcc rolling texture components are illustrated in Figure 5. Here, only the $\varphi_2 = 45$ deg section of Euler space is used, and the letters refer to the slip system notation employed in Table II. The product orientations lying outside this cross section are not included in these diagrams but are listed in Table IV. Also indicated on the diagrams are the variants that are eliminated from consideration by the residual stress rule (as discussed later). Finally, the symbols employed on the diagrams enable distinctions to be drawn between the systems carrying the largest amount of slip (full symbols), the second largest amount of slip (gray symbols), and light slip or no slip at all (open symbols). These diagrams are presented here so that they can be used to deduce the sources (in the austenite) of prominent orientations in experimental (bcc) textures.

C. *Effect of Grain Aspect Ratio and Crystal Growth Direction*

When an equiaxed microstructure is deformed under plane strain rolling conditions, the grains become elongated along the rolling direction and reduced in thickness, while their transverse dimensions remain unchanged. Thus, the microstructure becomes pancaked to an extent that depends on the reduction applied. For example, elongation ratios l_f/l_i of 3, 4, 5, and l0 correspond to rolling reductions of 67, 75, 80, and 90 pct, respectively. Similarly, the grain heights h are reduced by the inverse values of these ratios. The aspect ratios l/h in the longitudinal cross section therefore increase from 1.0 when the grains are equiaxed to $3^2 = 9$, $4^2 = 16$, $5^2 = 25$, and $10^2 = 100$ for the four reductions, respectively.

The effect of grain shape on variant selection has been investigated in the past without success. For instance, Davies and Bateman[11] considered the possibility that martensite plates could grow longer when parallel to the rolling plane. However, this idea was applied to *all* the 24 variants of the K–S transformation, so that the texture predicted in this way was exceptionally weak.

When the grain shape is highly directional, as in the case of the present pancaked grains, and the transformation is directional as well, there are appreciable consequences. It is clear, for example, that there is one or even two orders of magnitude more scope for growth along the RD than in the ND (vertical) direction. For similar reasons, growth along the RD will be favored over TD growth by factors of 3, 4, 5, and 10 for the four reductions considered previously. Thus, orientations associated with RD growth can be expected to be favored over the equivalent TD orientations, while both of these will be enormously favored over the ND orientations.

The favored (and retarded) orientations can be readily deduced from the K–S correspondence relations and the general observation that the favored growth direction is related to the ⟨111⟩ direction normal to the {111}-fcc plane involved in the correspondence relation.[19]

In order to determine the favored product orientations, it must first be noted that the ideal orientations forming the fcc rolling fiber have a ⟨111⟩ direction lying in the rolling (*i.e.*, ND) plane. For example, a ⟨111⟩ direction lies parallel to RD in the case of the {112}⟨111⟩ (or copper) component,

Table IVa. Characteristics of the 24 K–S Variants Arising from the Copper, Brass, and S Orientations*

			Copper (112) [$\bar{1}\bar{1}$1]						Brass (101) [$\bar{1}\bar{2}$1]						S (213) [$\bar{3}\bar{6}$4]					
Number	Axis	System	*hkl*	*uvw*	φ_1	Φ	φ_2	Activity	*hkl*	*uvw*	φ_1	Φ	φ_2	Activity	*hkl*	*uvw*	φ_1	Φ	φ_2	Activity
1	−1 −1 −2	−bIII	211	011	0	35	45	*000*	111	123	20	65	45	*000*	111	123	16	46	45	*000*
2	−1 1 2	−dIII	421	012	10	29	55	+1.4	211	113	21	42	52	+1.2	211	113	89	71	55	+1.7
3	1 −1 2	−cIII	421	012	7	20	52	−1.4	111	112	90	65	45	−0.4	211	113	21	31	55	−0.9
4	1 1 −2	−aIII	211	011	15	37	27	0	211	120	10	66	55	0	221	012	72	68	47	0
5	1 2 1	dII	421	012	9	32	18	0	211	113	28	36	54	0	221	114	84	77	49	0
6	1 −2 −1	bII	311	011	0	25	45	*000*	111	123	20	55	45	*000*	321	012	16	36	45	*000*
7	−1 2 −1	aII	321	012	64	72	53	−0.4	211	113	43	36	36	0	221	012	84	68	43	−0.4
8	−1 −2 1	cII	311	011	20	26	33	0	111	112	30	55	45	0	211	113	31	36	39	−0.04
9	−2 −1 −1	−cI	421	012	9	32	18	0	100	011	90	5	45	+0.4	411	011	30	21	13	0
10	−2 1 1	−aI	321	012	64	72	53	−0.4	100	011	34	10	17	−1.2	311	011	21	29	27	−0.5
11	2 −1 1	−bI	311	011	0	25	45	*000*	100	012	20	5	45	*000*	100	012	16	14	45	*000*
12	2 1 −1	−dI	311	011	20	26	33	0	100	012	31	87	10	0	411	011	17	16	19	−0.05
13	1 1 2	bIII	211	011	0	35	45	*000*	100	012	20	5	45	*000*	421	012	16	24	45	*000*
14	1 −1 −2	dIII	421	012	7	20	52	−1.4	100	011	34	10	17	−1.2	100	011	1	9	46	−1.7
15	−1 1 −2	cIII	421	012	10	29	55	+1.4	100	011	90	5	45	+0.4	311	011	0	18	49	+0.9
16	−1 −1 2	aIII	211	011	15	37	27	0	100	012	31	87	10	0	210	122	36	26	21	0
17	−1 −2 −1	−dII	210	120	72	33	19	0	211	113	43	36	36	0	210	121	75	31	2	0
18	−1 2 1	−bII	110	110	0	85	45	*000*	111	123	20	55	45	*000*	321	153	16	74	45	*000*
19	1 −2 1	−aII	210	120	81	26	4	+0.4	211	113	28	36	54	0	210	124	60	26	21	+0.4
20	1 2 −1	−cII	110	110	9	84	50	0	111	112	30	55	45	0	321	121	25	74	49	+0.04
21	2 1 1	cI	210	120	72	33	19	0	111	112	90	65	45	−0.4	211	113	42	38	36	0
22	2 −1 −1	aI	210	120	81	26	4	+0.4	211	113	21	42	52	+1.2	211	113	45	29	27	+0.5
23	−2 1 −1	bI	110	110	0	85	45	*000*	111	123	20	65	45	*000*	110	221	16	84	45	*000*
24	−2 −1 1	dI	110	110	9	84	50	0	211	120	10	66	55	0	110	110	7	85	52	+0.05

*Equivalent tables apply to the symmetry components of each parent orientation.

Table IVb. Characteristics of the 24 K–S Variants Arising from the Goss, Goss-Brass, Brass-S, and S Orientations*

	Goss (101) [0 $\bar{1}$ 0]						Goss-Brass (101) [$\bar{1}\,\bar{5}$ 1]						Brass-S (67, 17, 100) [$\bar{1}\,\bar{2}$ 1]						S-Copper (59, 43, 100) [$\bar{6}\,\bar{9}$, $\bar{1}\,0\,\bar{0}$, 83]					
Number	*hkl*	*uvw*	φ_1	Φ	φ_2	Activity	*hkl*	*uvw*	φ_1	Φ	φ_2	Activity	*hkl*	*uvw*	φ_1	Φ	φ_2	Activity	*hkl*	*uvw*	φ_1	Φ	φ_2	Activity
1	111	011	55	65	45	*000*	221	122	39	65	45	−0.01	111	123	41	60	45	*000*	322	011	8	41	46	*000*
2	211	011	45	66	55	+0.6	211	011	1	42	52	+1.0	332	113	87	65	40	+1.3	211	113	17	34	58	+1.6
3	111	011	55	65	45	*000*	332	023	71	65	45	−0.1	211	113	29	38	48	−0.7	421	012	14	25	55	−1.2
4	211	011	45	66	55	+0.6	211	113	30	42	38	+0.2	111	123	76	61	44	0	321	012	63	71	52	0
5	211	011	7	36	36	0	321	012	8	36	54	0	332	113	88	70	45	+0.001	321	012	75	79	54	0
6	111	011	5	55	45	*000*	111	123	21	55	45	0	221	122	24	42	38	*000*	311	011	8	30	46	*000*
7	211	011	7	36	36	0	321	133	23	36	36	0	332	113	33	47	49	−0.2	321	012	74	71	48	−0.4
8	111	011	5	55	45	*000*	111	123	11	55	45	0	211	113	26	67	52	0	211	153	25	31	37	−0.02
9	100	001	55	5	45	*000*	100	012	71	5	45	+0.1	411	011	21	15	25	+0.003	421	012	21	27	15	0
10	100	001	69	10	17	−0.6	310	131	53	10	17	−1.0	311	011	15	23	37	−1.1	211	011	14	35	27	−0.4
11	100	001	55	5	45	*000*	100	001	39	5	45	+0.01	100	012	11	9	15	*000*	411	011	10	20	44	*000*
12	100	001	69	10	17	−0.6	310	131	78	80	3	−0.2	310	135	32	75	3	0	411	011	15	21	29	−0.02
13	100	001	55	5	45	*000*	100	001	39	5	45	+0.01	421	012	6	19	59	*000*	311	011	9	30	44	*000*
14	100	001	69	10	17	−0.6	310	131	53	10	17	−1.0	100	011	40	82	1	−1.3	411	011	1	15	39	−1.6
15	100	001	55	5	45	*000*	100	012	71	5	45	+0.1	411	011	21	15	25	+0.7	421	012	3	23	54	+1.2
16	100	001	69	10	17	−0.6	310	131	78	80	3	−0.2	310	132	32	19	28	0	321	133	26	32	24	0
17	211	011	7	36	36	0	321	133	23	36	36	0	210	124	61	27	15	−0.001	320	230	81	59	6	0
18	111	011	5	55	45	*000*	111	123	21	55	45	0	321	153	49	45	32	*000*	331	110	9	80	45	*000*
19	211	011	7	36	36	0	321	012	8	36	54	0	311	114	42	24	38	+0.2	320	230	79	26	8	+0.4
20	111	011	5	55	45	*000*	111	123	11	55	45	0	211	113	26	67	52	0	321	351	18	79	49	+0.02
21	111	011	55	65	45	*000*	332	023	71	65	45	−0.1	211	113	29	38	48	−0.003	321	351	56	35	27	0
22	211	011	45	66	55	+0.6	211	011	1	42	52	+1.0	211	113	29	29	42	+1.1	210	124	63	27	15	+0.4
23	111	011	55	65	45	*000*	221	122	39	65	45	−0.01	321	121	18	78	50	*000*	110	110	9	90	45	*000*
24	211	011	45	66	55	+0.6	211	113	30	42	38	+0.2	321	153	65	34	19	0	110	110	0	90	39	+0.02

*Equivalent tables apply to the symmetry components of each parent orientation. Note that the rotation axis and slip system associated with each variant number in Table IVa are also applicable here.

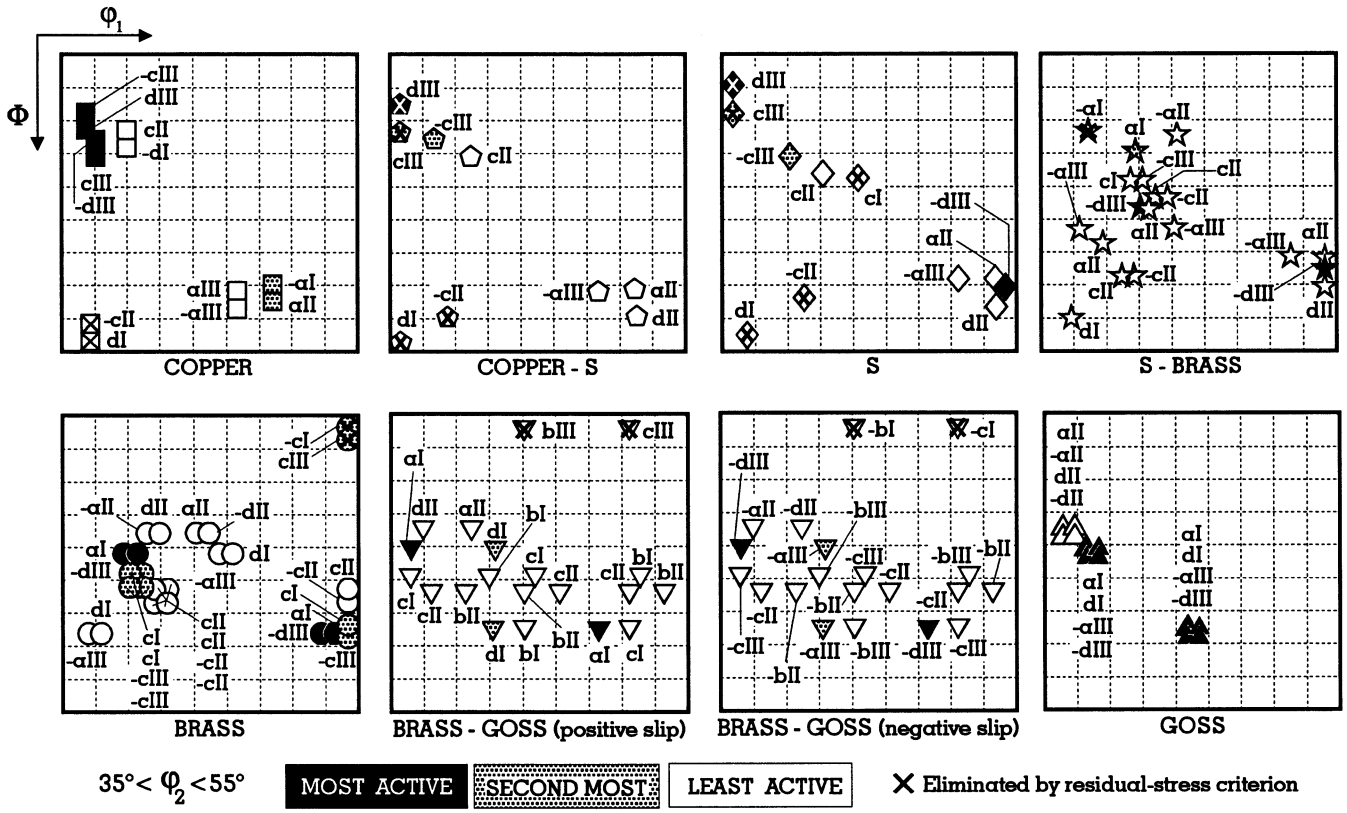

Fig. 5—Product orientations associated with the slip systems lying in active planes for each of the seven parent components. All variants in the range 35 deg ≤ φ_2 ≤ 55 deg are included. For clarity, the brass-Goss products are separated into two distinct diagrams. The slip system notation corresponds to that of Table II.

while a ⟨111⟩ direction is aligned with TD in the case of the {110}⟨112⟩ (or brass) component. For the Goss ({110}⟨001⟩), S ({123}⟨634⟩), and S-copper components, there is a ⟨111⟩ vector once again lying in the horizontal plane, but it is inclined at angles of 54.7, 16.0, and 8.6 deg to the RD. The {111} planes that are normal to these particular ⟨111⟩ vectors are thus all ''vertical'' planes and are therefore unable to carry any slip during rolling. That is, these correspond to the various *inactive* planes defined in Section B. Each inactive plane when employed in the K–S relationship leads in turn to up to six possible product orientations, corresponding to the plus or minus 90 deg rotations about the three ⟨112⟩ axes lying in that plane.

Variants favored by the geometry of planar growth

The variants that satisfy the geometric requirements for growth along the high aspect ratio directions of pancaked grains are identified in Figure 6 for the seven exact parent orientations. (Here, the Bishop and Hill slip system notation is once again employed.) However, a few of these variants are not free to grow because of the restrictions imposed by the residual stress condition described subsequently. These are identified as such in Figure 6. The variants that remain can then be classified according to their growth directions, where the RD is the most favoured and the TD the least favored planar direction (Table V).

It is clear from the preceding analysis that a possible reason for the prominence of the {311}⟨011⟩ and {211}⟨011⟩ transformation texture components is that these are the *only ones* that are perfectly aligned for growth along the RD direction. Less favored are the approximate {111}⟨123⟩ components that are expected to grow in the TD direction (and which form from the fcc brass component). The approximate {111}⟨011⟩ components that arise from the Goss parent orientation are also less favored, but are expected to be of low intensity in the final texture because the Goss and Goss-brass components normally have the lowest intensities in the rolling fiber.[33] The transformed brass-S, S, and S-copper growth components in turn are also expected to play less significant roles, because their low symmetries do not lead to any variant overlap or multiplicity.

D. *Effect of Residual Stress on Variant Selection*

Several researchers have already shown that the presence of an applied or existing stress has an effect on the transformation texture components.[34,35] Of interest in the present context is that residual stresses remain in deformed materials after unloading; these are associated with the previous deformation path. Here, a growth condition is employed,[18] based on the idea that, after rolling, each grain embedded in the austenite matrix is subject to a residual stress σ'_{ij} that depends on the difference between (1) the stress applied to the polycrystal during the last rolling pass and (2) the stress required to cause the grain to yield, also in the last rolling pass.

This subtraction is represented by the relation $\sigma'_{ij} = S_{ij} - \sigma_{ij}$, where σ_{ij} is the single crystal yield stress calculated using the Bishop and Hill[26] analysis and S_{ij} is the stress obtained from the upper bound random polycrystal yield locus for the same strain path. No work hardening or strain

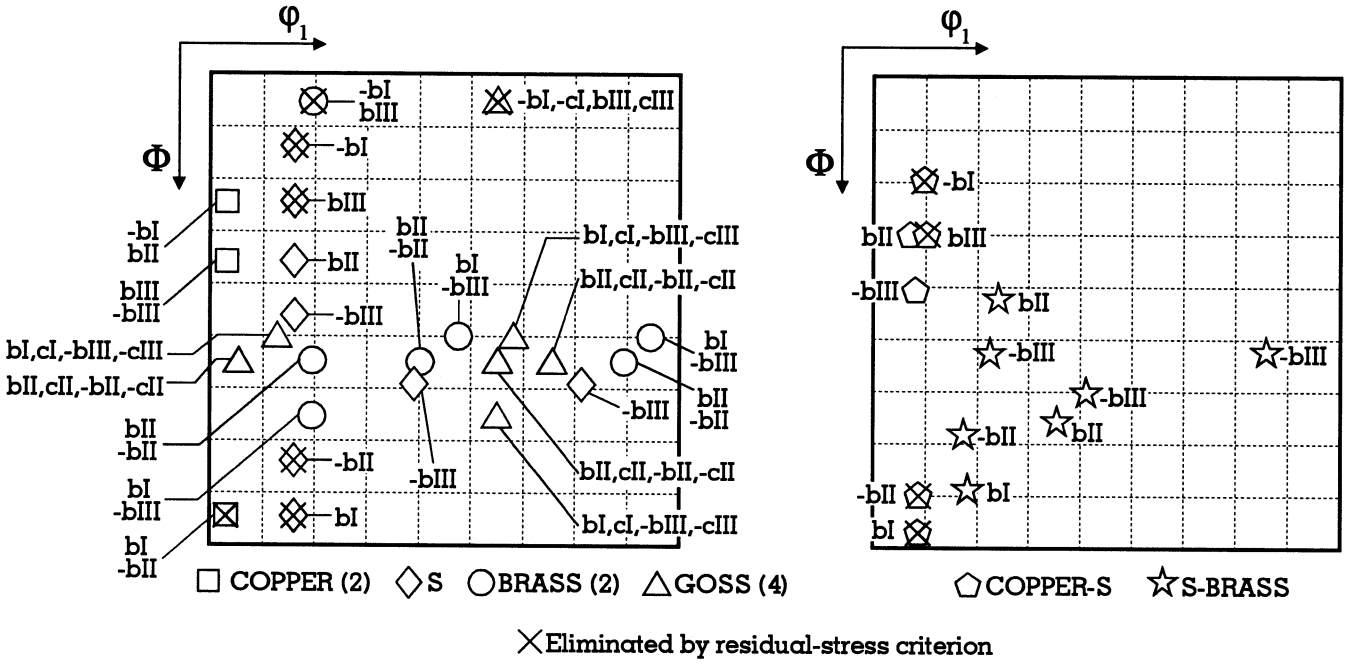

Fig. 6—Product orientations and slip systems associated with the totally inactive planes for six of the seven parent orientations. All variants in the range 35 deg ≤ φ_2 ≤ 55 deg are included. For the copper, brass, and Goss orientations, each symbol represents two, two, and four variants, respectively.

Table V. Planar Growth Variants

Growth Direction	Source in Rolling Fiber	Variants (Bishop and Hill Notation)	Approximate Miller Indices
RD (highly favored)	copper	bII, −bI,	{311} ⟨011⟩
		bIII, −bIII	{211} ⟨011⟩
Diagonal (mildly favored)	S	−bI, bII, bIII, −bIII	{*hkl*} ⟨012⟩
	Goss	bII, −bII, cII, −cII,	{111} ⟨011⟩
		bI, cI, −bIII, −cIII	near {111} ⟨011⟩
TD (least favored)	brass	bI, −bIII,	near {111} ⟨123⟩
		bII, −bII	{111} ⟨123⟩

history due to previous rolling passes is therefore taken into account.

The rule can be stated as follows: ''those variants are favored which reduce the residual stress in the matrix surrounding a given parent grain.'' Conversely, those variants are eliminated which *increase* the residual stress and therefore increase the energy stored in the matrix.

In order to simplify the analysis and to be able to select the variants that will grow using a single parameter, the work ΔW resulting from the action of the residual stress σ'_{ij} on the transformation strain ε_{ij} was calculated. Positive values of the work were considered here to aid the transformation, and therefore, the product orientations resulting from the satisfaction of the following condition were the ones selected:

$$\Delta W = \sigma'_{ij} \cdot \varepsilon_{ij} \geq 0 \qquad [1]$$

Here, ε_{ij} is taken to be the Bain strain associated with fcc and bcc lattice parameters of 0.361 and 0.286 nm, respectively. This choice of parameters ensures that no volume change takes place during transformation (in practice, it is about 2 pct), an approach that again simplifies the analysis.

The term ε_{ij} assumes three different tensor forms according to the particular ⟨100⟩ parent axis that is aligned with its negative normal (*i.e.*, contraction) component. Each of the ⟨100⟩ axes is in turn related to eight of the 24 ⟨112⟩ rotation axes shown in Table II and Figure 2(b). (In the figure, only the positive axes are illustrated.) The use of the work rule therefore leads to the elimination of the variants that *increase* the stored energy in the matrix. Conversely, the rule leads to the selection of the product orientations that *decrease* the energy and are hence allowed to grow. Table VI shows the residual stress work (in units of $\sqrt{6}\tau_c$) calculated for each of the seven parent components using Eq. [1], but with the Bain strain (0.24) reduced by an order of magnitude (to 0.024). The eight variants that correspond to each ⟨100⟩ contraction axis are numbered according to the nomenclature used in the first column of Table IV. There is a maximum of three different values of work per parent orientation, since, as mentioned earlier, the residual stress may be different for each possible contraction axis. The contraction axes that are either selected (S) or eliminated (E) in this way are also identified.

Also listed in Table VI are the differences between the maximum and minimum work values, expressed in kJ/mole. (Here, τ_c was set equal to 100 MPa.) These range from about 1 kJ/mole for the Goss orientation, which has low ''selectivity'' according to this criterion, to ≈40 to 52

Table VI. Selectivity Characteristics of the Seven Rolling Fiber Components*

Parent Orientation	Contraction Axis	Product Variant Number	Residual Stress Work	Selected or Eliminated	Selectivity + − (−) (kJ/mole)
Copper	⟨100⟩	1 through 8	+0.044	S	9
	⟨010⟩	9 through 16	+0.044	S	
	⟨001⟩	17 through 24	−0.085	E	
Copper-S	⟨100⟩	1 through 8	+0.140	S	16
	⟨010⟩	9 through 16	−0.054	E	
	⟨001⟩	17 through 24	−0.085	E	
S	⟨100⟩	1 through 8	+0.210	S	26
	⟨010⟩	9 through 16	−0.150	E	
	⟨001⟩	17 through 24	−0.061	E	
S-Brass	⟨100⟩	1 through 8	+0.073	S	45
	⟨010⟩	9 through 16	−0.355	E	
	⟨001⟩	17 through 24	+0.281	S	
Brass	⟨100⟩	1 through 8	+0.183	S	40
	⟨010⟩	9 through 16	−0.365	E	
	⟨001⟩	17 through 24	+0.183	S	
Brass-Goss	⟨100⟩	1 through 8	+0.245	S	52
	⟨010⟩	9 through 16	−0.490	E	
	⟨001⟩	17 through 24	+0.245	S	
Goss	⟨100⟩	1 through 8	+0.005	S	1
	⟨010⟩	9 through 16	−0.010	E	
	⟨001⟩	17 through 24	+0.005	S	

*Here, the residual stress work is expressed in units of $\sqrt{6}\ \tau_c$, and the selectivity was derived on the basis of τ_c = 100 MPa.

kJ/mole in the vicinity of the brass and neighboring components, which therefore have high selectivity. Finally, it should be added that these energies are comparable with the free energies that drive the γ-to-α transformation in iron-carbon alloys at about 100 °C to 200 °C below the A_{c3}. The latter can be estimated to fall in the range −100 to −300 kJ/mole in the present low C steels.[36] Thus, it appears that the free energy of transformation can be modified sufficiently by relaxation of the internal stresses as described previously (or by their increase when contraction is attempted along a direction where the residual stress is tensile) to affect the kinetics of formation of alternative variants.

It should be noted that the present criterion is based solely on the orientation of the parent grain and not on that of the nucleus. As a result, a product orientation that can form from more than one parent orientation can be unable to grow from the one but be encouraged to do so from another.

The residual stress distributions pertaining to all seven parent orientations are presented in Figure 7. Here, the specimen axes are employed and only the normal components of the stress tensor are represented. These values were calculated by assuming that the hydrostatic stress is zero in each case. The positions of the three ⟨100⟩ parent axes are also shown. The ⟨100⟩ axes that are selected as the contraction axes are those that lie in the regions of lowest absolute stress.

The preceding results are collected and displayed in Figure 8. In this diagram, both the *permissible* as well as the unfavorable contraction axes are plotted. Additional points have been added for all but the Goss orientation so as to respect the requirements for orthorhombic symmetry. It is evident from the figure that the unfavorable contraction axes lie within about 40 deg of the RD pole. Conversely, the *permissible* contraction axes are located along the TD-ND plane or within about 45 deg of the two TD poles.

The important effect of eliminating the contraction axes in the neighborhood of the RD poles from consideration is that certain variants, which are not in fact observed (or are only present at low intensities), are also eliminated from texture predictions. These include the {100}⟨001⟩ (and near {100}⟨001⟩) expected from the Goss, the {100}⟨011⟩ and {100}⟨012⟩ that are expected to form from the brass, the {110}⟨110⟩ and {210}⟨120⟩ that would otherwise form from the copper, and the near {110}⟨110⟩ orientations arising from the S.[4,13] As this mechanism of variant selection is linked to the presence of residual stresses in the material, it can, however, be expected to work less efficiently if there is appreciable stress relaxation prior to transformation.

E. *Variant Selection Using a Combination of Slip Nucleation, Planar Growth, and Residual Stress-Based Criteria*

We can now combine the product orientations selected by the slip activity and planar growth criteria to produce the transformed texture. The first step is to remove from these groups all the product orientations that do not satisfy the residual stress criterion. This was easily done by selecting only the variants that led to positive values of the work, as indicated previously.

Now, a partial product texture can be obtained from the orientations resulting from the slip activity criterion alone. In order to do this, the product orientations associated with the most active parent slip systems were fitted by Gaussian functions to produce the ODF section shown in Figure 9(a). The same was done with the orientations resulting from the

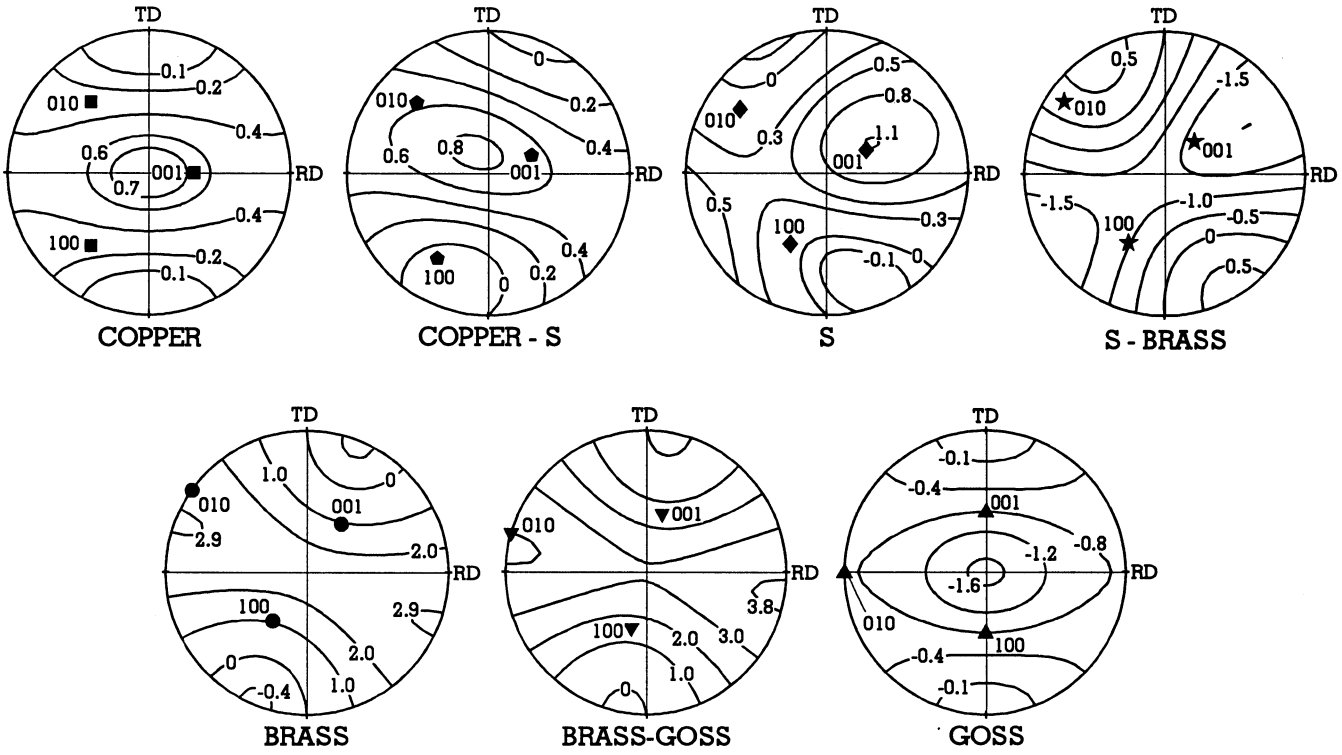

Fig. 7—Stereographic representation, in the sample reference frame, of the residual stress distribution that applies to each of the seven parent components. The positions of the three ⟨100⟩ poles are also indicated.

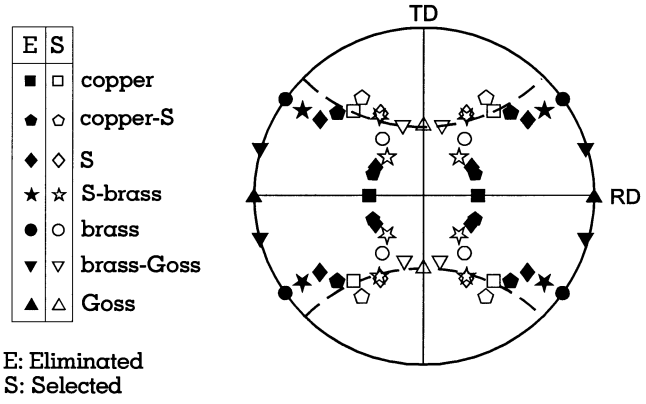

Fig. 8—Stereographic representation, in the sample reference system, of the locations of the ⟨100⟩ poles of the seven parent orientations. Here, the residual stress criterion was employed to eliminate (E) or select (S) the various possible contraction axes.

second most active systems, yielding the ODF section in Figure 9(b). Figure 9(c) is a combination of these two ODFs in the ratio 4:1.

It is evident from the figure that this approach is able to simulate many of the features of the experimental textures of Figure 4. For example, the location and intensity of the {332}⟨113⟩ component of the TD fiber are *accurately* reproduced. As pointed out previously, this orientation is principally derived from the brass component of the austenite rolling texture. By contrast, the intensities along the ⟨110⟩‖RD fiber (left side of the ODF) are much too low, particularly in the vicinity of $\phi = 25$ deg ({311}⟨011⟩) and $\phi = 35$ deg ({211}⟨011⟩). These are mainly formed from the austenite copper orientation. As will be seen subsequently, the reasons for this differential behavior lie in the morphological characteristics of the austenite microstructure immediately before the transformation;[19] in particular, the effect of grain shape on the growth rate of the nuclei will now be analyzed in detail.

Effect of planar growth components

A simulated ODF representing the expected contribution of the planar growth orientations to the overall ODF is presented in Figure 10. In the present case, the pancaked grains were assumed to have aspect ratios of 7:1 (length:width), which corresponds to a rolling reduction of 84 pct. Here, relative weights of 7:6.4:1.62:1:1:1.22 were employed for the copper, copper-S, S, S-brass, brass, and Goss product orientations, respectively. (The brass-Goss orientation was not included in this group because of its low intensity and low symmetry.) These weights were obtained from the angle α between the ⟨111⟩ normal to the inactive (vertical) slip plane and the RD using the expression $1/\sin\alpha$. For $\alpha = 0$ deg (the copper orientation), an arbitrary weight of 7 was chosen. The key contribution made by the two transformed copper components selected in this way is readily evident. The less favored transformed brass and transformed Goss components can be seen to contribute to the ⟨111⟩‖ND fiber (which includes orientations with a ⟨111⟩ axis parallel to the ND). This fiber will be strong when the copper component is significantly weaker than the brass and planar growth continues to play an important role.

It is clear from the preceding considerations that, in an experimental texture, the actual strengths of the two ⟨110⟩‖RD components, {311}⟨011⟩ and {211}⟨011⟩, can be expected to depend on the aspect ratios of the pancaked grains and, therefore, on the strain accumulated below the T_{nr} in the rolling schedule employed. Higher pancaking strains also increase the intensity of the copper component

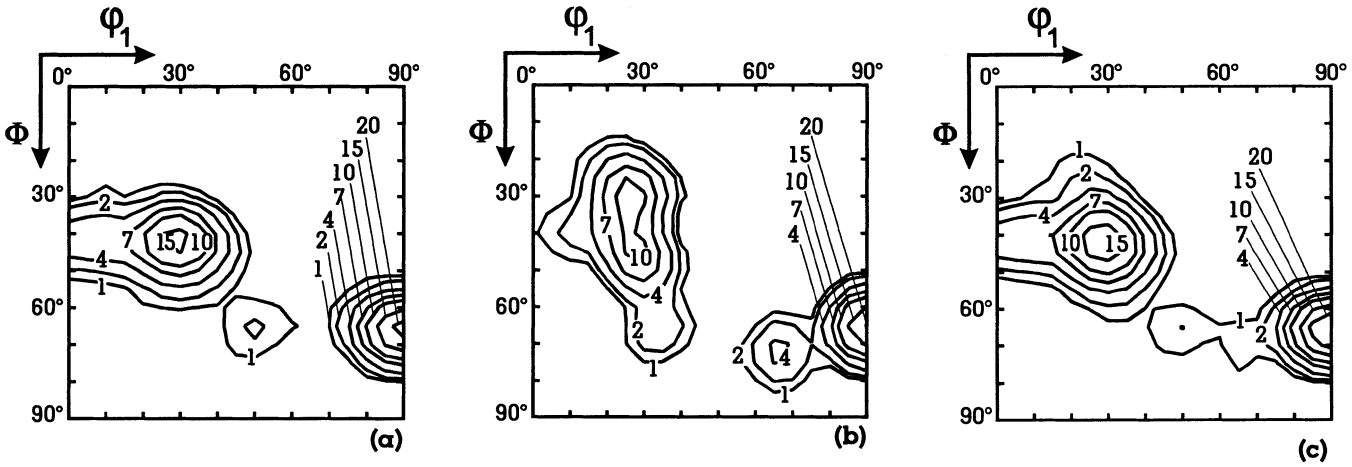

Fig. 9—φ_2 = 45 deg ODF sections showing (*a*) the most active and (*b*) the second most active K–S variants. Gaussian function fitting. (*c*) Combination of (a) and (b) in a ratio of 4:1.

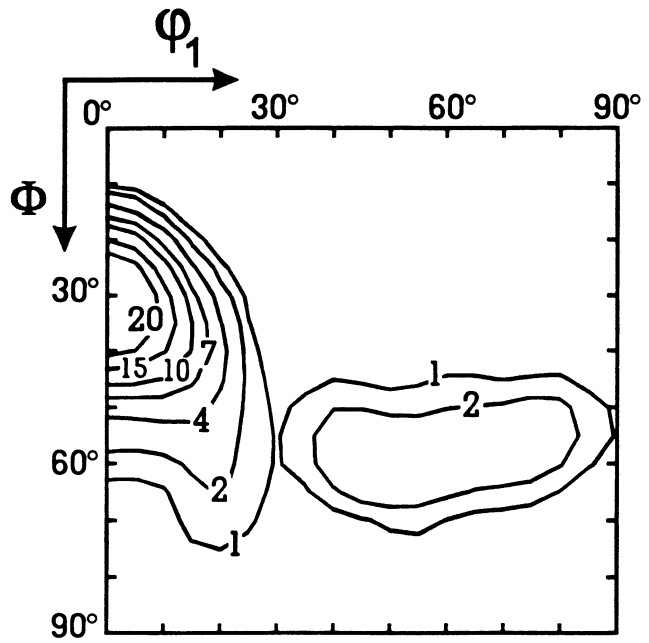

Fig. 10—φ_2 = 45 deg ODF section showing the variants that correspond to the totally inactive slip systems of the Cu, Cu-S, S, S-Brass, Brass, and Goss orientations. Gaussian function fitting.

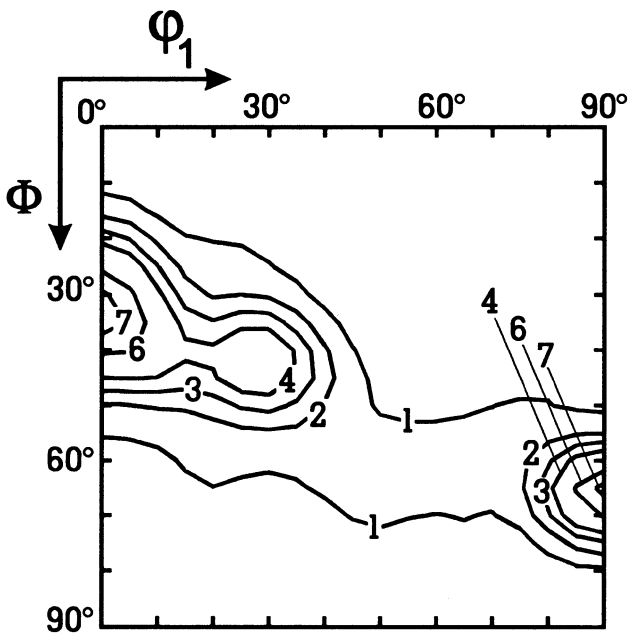

Fig. 11—Combination of Figs. 9(c) and 10 in a ratio of 5:4.

of the parent fcc rolling fiber and, therefore, contribute in a second way to increasing the intensities of the two latter orientations.

It is now possible to combine the ODF of Figure 10, calculated using the concept of enhanced growth along the planar directions, with that of Figure 9(c) which represents the graduated effect on nucleation of shear on the active slip planes. The result obtained in this way is presented in Figure 11. Here, it can be seen that all the important features of the ODFs of Figure 4 have been reproduced. At this stage of model development, faster and slower cooling rates can only be simulated by adjusting the ''weights'' used to derive Figure 9(c); these can be considered to represent the relative dislocation densities associated with the three classes of slip system on the active slip planes that can be influenced by the extent of recovery. Similarly, differences in the amounts of pancaking strain can be taken into account by varying the aspect ratio factors employed to calculate Figure 10.

Use of the present rule for the prediction of complete textures requires a more elaborate weighting system than the one described briefly earlier. In this case, the original intensity of each parent orientation must be taken into account, together with the number of possible product variants of a given orientation, the four (or more) levels of slip activity outlined here, as well as the effect of the other growth criteria discussed earlier. The results obtained from such a more complex approach will be presented in a forthcoming publication.

IV. DISCUSSION

Experimental transformation textures reveal the presence of considerably fewer variants than are called for by the K–S relationship. As shown in the subsection to Section III–A, the prediction of transformation textures without

variant selection leads to results that differ both qualitatively and quantitatively from the observations. This has led to the clear conclusion that variant selection mechanisms are active during phase transformation. Many selection criteria were tested in the past, none of which has been completely successful.

In the present work, a model is proposed that takes into account the microstructural condition of the austenite immediately before transformation. Both the dislocation distribution and the grain morphology are considered to influence the final texture. Two important mechanisms are identified that account for the varying intensities of the most prominent orientations in the transformation texture: these are the slip activity-based nucleation rule and the grain aspect ratio growth rule. As seen in section III·B, the former governs the intensity of the $\{332\}\langle 113\rangle$ and $\{211\}\langle 113\rangle$ bcc components, which are mainly derived from the brass component of the parent texture.

It is therefore clear that the intensities of the transformed brass components are sensitive to the pattern and amount of prior slip and, as a consequence, to such variables as cooling rate, since this affects the extent of recovery. Conversely, it can be postulated that the lower the dislocation density when the transformation begins (*i.e.*, the lower the cooling rate), the less effective is this mode of variant selection, and therefore the lower the intensities of the transformed brass components. This had already been noted by Inagaki[1] and Yutori and Ogawa,[2] who did not however explain their observations.

The product orientations selected on the basis of slip activity include a number of components that are not observed experimentally. These include the cube, $\{100\}\langle 001\rangle$, which forms from the Goss, and the rotated Goss, $\{110\}\langle 110\rangle$, which forms from the copper. However, these are eliminated by the residual stress condition described earlier. (In the present instance, variants 9 through 16 are ruled out in this way in the case of the Goss and brass parent orientations, as are variants 17 to 24 in the case of the copper.)

In contrast to the transformed brass components, the intensities of which are inversely related to the amount of recovery prior to transformation, the bcc $\{211\}$-$\{311\}\langle 011\rangle$ orientations are formed from the fcc copper component. As shown in Section III–C, the $\{111\}$ correspondence plane of this component remains inactive during prior straining; as it contains no active burgers vectors, the volume fractions of the product grains cannot be sensitive to either cooling rate or the amount of previous recovery. Their intensities will increase with the extent of grain pancaking and, therefore, with the amount of reduction applied below the recrystallization-stop temperature. The physical reason for preferential growth along the RD is as yet unknown. It is, however, under current investigation and will be the subject of a future article.

An interesting feature of the present approach is the necessity of including a further criterion related to the release of stored energy during phase transformation. In Section III–D, a simplified calculation was used, which was based on two basic assumptions: (1) that each grain is surrounded by a uniform distribution of orientations (this justifies the use of the random yield locus to represent the contribution of the matrix to the residual stress field); and (2) that the transformation strain associated with each K–S variant in a group of eight (Figure 1) can be represented by the Bain strain pertaining to the average for that group.

With the aid of these assumptions, the remaining ''unwanted'' orientations were eliminated, as discussed in Section III–D. It should be noted, however, that this criterion is also sensitive to dislocation density and, as a consequence, to cooling rate and the extent of recovery. It is not applicable to a recrystallized parent matrix, in which such residual stresses are absent.

V. CONCLUSIONS

1. Experimental transformation textures are more intense and reveal the presence of considerably fewer variants than called for by the K–S relationship. This leads to the clear conclusion that variant selection is taking place.
2. When pancaked austenite grains are consumed by retreating along $\langle 111\rangle$ directions, those with directions lying in the rolling (ND) plane are particularly favored. The bcc orientations produced in this way are associated with the *vertical* fcc $\{111\}$ planes that are associated with the fcc rolling fiber.
3. The extent of grain pancaking can be quantified in terms of the grain aspect ratio, which is directly related to the rolling reductions applied below the T_{nr} and therefore to the pancaking strain. The aspect ratio is a good measure of the extent to which growth along the RD direction will be favored when plane strain rolling has taken place. The two bcc orientations whose intensities are particularly promoted in this way are the $\{311\}\langle 011\rangle$ and $\{211\}\langle 011\rangle$, both of which are formed from the copper component of the rolling fiber. (When the brass component is significantly more intense than the copper, the $\langle 111\rangle \| \mathrm{ND}$ fiber will be promoted instead.)
4. The intensities of the preceding two transformed copper components are not affected by the slip activity during prior rolling or by the dislocation density. This is because of the absence of slip activity on the vertical $\{111\}$ planes that are participating in the transformation.
5. Nucleation of the $\{332\}\langle 113\rangle$ and $\{211\}\langle 113\rangle$ transformed brass components is associated with slip activity on particular $\{111\}$ planes. The loss of dislocations on these planes will lead to a decrease in the extent of variant selection in favor of these two orientations. This can explain why the intensities of the transformed brass components are affected by cooling rate and by the extent of recovery prior to transformation.
6. After rolling, there is a local residual stress that corresponds to the difference between the applied polycrystal yield stress and the flow stress of the grain under consideration. During transformation, the relaxation of this residual stress acts to favor certain possible Bain contraction axes over others and therefore to the derivation of a residual stress rule. The role of this rule is to *reject* some of the variants selected by both the planar growth and slip-based criteria; this applies to all of the $\{110\}\langle 110\rangle$ and $\{100\}\langle uvw\rangle$ orientations otherwise chosen by the latter two criteria.
7. Experimentally observed transformation textures can be readily reproduced with the aid of three variant selection criteria. These involve (1) a slip activity *nucleation* cri-

terion; (2) a grain aspect ratio planar *growth* criterion and (3) a residual stress-based *growth* criterion.

ACKNOWLEDGMENTS

The authors are grateful to the Natural Sciences and Engineering Research Council of Canada (NSERC) and the Canadian Steel Industry Research Association (CSIRA) for financial support. CSDCV is indebted to the Instituto Militar de Engenharia (IME) (Rio de Janeiro, Brazil) for granting a period of sabbatical leave, during which this research was completed.

REFERENCES

1. H. Inagaki: *Proc. 6th Int. Conf. on Textures of Materials*, The Iron and Steel Institute of Japan, Tokyo, 1981, vol. 1, pp. 149-63.
2. T. Yutori and R. Ogawa: *Proc. 6th Int. Conf. on Textures of Materials*, The Iron and Steel Institute of Japan, Tokyo, 1981, vol. 1, pp. 669-79.
3. R.K. Ray and J.J. Jonas: *Int. Mater. Rev.*, 1990, vol. 35 (1), pp. 1-36.
4. R.K. Ray, J.J. Jonas, M.P. Butrón-Guillén, and J. Savoie: *Iron Steel Inst. Jpn. Int.*, 1994, vol. 34 (12), pp. 927-42.
5. A. Jones and B. Walker: *Met. Sci.*, 1974, vol. 8, pp. 397-406.
6. P. Chapellier, R.K. Ray, and J.J. Jonas: *Acta Metall. Mater.*, 1990, vol. 38 (8), pp. 1475-90.
7. R.J. Roe: *J. Appl. Phys.*, 1965, vol. 36, pp. 2024-31.
8. G.J. Davies, J.S. Kallend, and P.P. Morris: *Acta Metall.*, 1976, vol. 24, pp. 159-72.
9. C.M. Sargent: *Scripta Metall.*, 1974, vol. 8, pp. 821-24.
10. R.M. Bateman and G.J. Davies: *Proc. 6th Int. Conf. on Textures of Materials*, The Iron and Steel Institute of Japan, Tokyo, 1981, vol. 1, pp. 690-702.
11. G.J. Davies and R.M. Bateman: *Proc. 6th Int. Conf. on Textures of Materials*, The Iron and Steel Institute of Japan, Tokyo, 1981, vol. 1, pp. 132-48.
12. H. Inagaki: *Z. Metallkd.*, 1984, vol. 75, pp. 510-16.
13. M.P. Butrón-Guillén, J.J. Jonas, and R.K. Ray: *Acta Metall. Mater.*, 1994, vol. 42, pp. 3615-27.
14. K. Haslam, T. Coleman, D. Dilieu, and I.L. Dillamore: *Proc. 3rd Int. Conf. on Textures of Materials*, Société Française de Métallurgie, Nancy, 1973, pp. 369-81.
15. J.C. Bokros and E.R. Parker: *Acta Metallurgica*, Vol. 11 (1963) pp. 1291-1301.
16. C.S. Da Costa Viana, M.P. Butrón-Guillén, and J.J. Jonas: in *Textures and Microstructures*, H. Hu Special Issue, 1996, vols. 26–27, pp. 599-610.
17. M.P. Butrón-Guillén, C.S. Da Costa Viana, and J.J. Jonas: *Proc. 11th Int. Conf. on Textures of Materials*, Xian, China, 1996, vol. 1, pp. 604-09.
18. C.S. Da Costa Viana, M.P. Butrón-Guillén, and J.J. Jonas: *Proc. 11th Int. Conf. on Textures of Materials*, Xian, China, International Academic Publishers, Beijing, China, 1996, vol. 1, pp. 610-15.
19. J.J. Jonas, M.P. Butrón-Guillén, and C.S. Da Costa Viana: *Proc. 11th Int. Conf. on Textures of Materials*, Xian, China, International Academic Publishers, Beijing, China, 1996, vol. 1, pp. 575-91.
20. E.C. Bain: *Trans. AIME*, 1924, vol. 70, pp. 25-35.
21. G. von Kurdjumov and G. Sachs: *Z. Phys.*, 1930, Bd. 64, pp. 325-43.
22. Z. Nishiyama: *Sci. Rep. Tohoku Imperial Univ.*, 1936, vol. 25, pp. 94-103.
23. G. Wassermann: *Arch. Eisenhúttenwes.*, 1933, vol. 6, pp. 347-51.
24. W.P. Liu and H.J. Bunge: *Mater. Lett.*, 1991, vol. 10, pp. 336-43.
25. E. Furubayashi, H. Miyaji, and M. Nobuki: *Trans. Iron Steel Inst. Jpn.*, 1987, vol. 27, pp. 513-19.
26. J.F. Bishop and R. Hill: *Phil. Mag.*, 1951, vol. 42, pp. 414-27 and 1298-1307.
27. P.M. Kelly and J. Nutting: *J. Iron Steel Inst.*, 1961, vol. 197, pp. 199-210.
28. C.J. Alstetter and C.M. Wayman: *Acta Metall.*, 1962, vol. 10, p. 992.
29. A. Akbarzadeh and J.J. Jonas: *Proc. Thermomechanical Processing, Theory, Modelling and Practice*, Stockholm, 1996, in press.
30. M.P. Butrón-Guillén: PhD Thesis, McGill University, Montreal, 1995.
31. G. Brückner, W. Aretz, and G. Gottstein: *Proc. 11th Int. Conf. on Textures of Materials*, Xian, China, International Academic Publishers, Beijing, China, Ed. by Z. Liang, L. Zuo and Y. Chu. 1996, vol. 1, pp. 592-97.
32. Y. Zhou, K.W. Neale, and L.S. Tóth: *Acta Metall. Mater.*, 1991, vol. 39, pp. 2921-30.
33. J. Savoie, R.K. Ray, M.P. Butrón-Guillén, and J.J. Jonas: *Acta Metall. Mater.*, 1993, vol. 42, pp. 2511-23.
34. G.H. Olsen and W.A. Jesser: *Acta Metall.*, 1971, vol. 19, pp. 1009-14 and 1299-1302.
35. G. Stone and G. Thomas: *Metall. Trans.*, 1974, vol. 5, pp. 2095-2102.
36. R. Hultgren, P.D. Desai, D.T. Hawkins, M. Gleiser, K.K. Kelley, and D.D. Wagman: *Selected Values of the Thermodynamic Properties of the Elements*, ASM, Metals Park, OH, 1973, pp. 180-91.